Cancer Cell International

RESEARCH

Open Access

Inhibiting Pyk2/Src expression by miR-23b-3p suppressed liver cancer stem cell function and hepatic carcinoma progression

Meng Sha[1†], Jiang Zhang[1†], Jin-kai Liu[1], Xiao-ye Qu[1], Chuan Shen[1], Ying Tong[1] and Jie Cao[1*]

Abstract

Background Liver cancer stem cells (LCSCs) are critical drivers of metastasis and chemoresistance in hepatocellular carcinoma (HCC). Proline-rich tyrosine kinase 2 (Pyk2) has been implicated in tumor progression, but its role in LCSC stemness and HCC malignancy remains unclear. This study explores the effects of Pyk2 and its regulation by miR-23b-3p on LCSC function and HCC progression.

Methods LCSCs were enriched from HepG2 and HCCLM3 cell lines, and Pyk2 knockdown was induced through siRNA transfection, with or without miR-23b-3p inhibitor co-transfection. We assessed cell proliferation, sphere formation, migration, invasion, and chemosensitivity. Stemness markers (Nanog, Oct4, Sox2, KLF4, and Bmi1) and Pyk2/Src signaling were analyzed via RT-qPCR, Western blotting, and immunohistochemistry. In vivo, tumor growth and Pyk2/Src expressions were evaluated in a BALB/c mouse xenograft model.

Results Pyk2 expression was significantly elevated in the identified LCSCs compared to the parental HCCs. Pyk2 knockdown significantly suppressed the LCSCs proliferation, sphere formation, migration, invasion, and enhanced chemosensitivity. The expression of stemness markers and miR-23b-3p was significantly inhibited in HCCLM3-LCSC^{siPyk2} cells. miR-23b-3p inhibition restored Pyk2 level and Src phosphorylation, reversing the suppressive effects of Pyk2 knockdown. In BALB/c mice, tumor volume, weight, and Pyk2/Src expressions were significantly elevated in HCCLM3-LCSC and HCCLM3-LCSC^{siPyk2}+miR-23b-3p inhibitor groups comparing to HCCLM3/HCCLM3-LCSC^{siPyk2} groups, whereas were even heightened in the HCCLM3-LCSC + miR-23b-3p inhibitor group.

Conclusions Inhibiting Pyk2/Src expression by miR-23b-3p suppressed LCSCs function and aggravated HCC progression.

Trial registration Not applicable.

Keywords Hepatocellular carcinoma, Liver cancer stem cells, Proline-rich tyrosine kinase 2, miR-23b-3p, Src

†Meng Sha and Jiang Zhang contributed equally to the present work.

*Correspondence:
Jie Cao
caojie@renji.com; caojie9-10@163.com
[1]Department of Liver Surgery, Renji Hospital, School of Medicine, Shanghai Jiao Tong University, 160 Pujian Road, Shanghai 200127, China

Background

Hepatocellular carcinoma (HCC), commonly known as liver cancer, is one of the most prevalent malignant tumors worldwide, ranking second in cancer-related mortality [1]. Despite the continuous advancements in liver cancer diagnosis and treatment, the clinical management of HCC remains challenging. Conventional radiotherapy, chemotherapy, transarterial chemoembolization (TACE), or targeted therapy with sorafenib are commonly employed in the treatment of primary HCC [2, 3]. However, liver cancer is highly resistant to radiotherapy and chemotherapy, and the efficacy of TACE and sorafenib is suboptimal. The 5-year recurrence rate after surgical resection is as high as 50–60%, with disease recurrence and metastasis being the major obstacles in improving the long-term prognosis of HCC patients [4]. Therefore, there is an urgent need to explore new strategies and identify more effective therapeutic approaches to tackle this devastating disease.

It is well-established that liver cancer stem cells (LCSCs) are closely related to the recurrence, metastasis, and chemotherapy resistance of HCC [5]. The tumor stem cell hypothesis proposes that tumors contain a small population of self-renewing, multipotent tumor-initiating cells that are critical for tumor relapse and drug resistance, and have been identified in various cancers including acute myeloid leukemia, breast cancer, and brain tumors [6–8]. Increasing evidence indicates that LCSCs exhibits self-renewal capacity and multi-lineage differentiation potential, which play a critical role in the initiation, progression, recurrence, and drug resistance of HCC [9]. The aberration of microRNAs, long non-coding RNAs, epigenetic/transcription/metabolism regulators, and others contribute to the stemness of HCC [10]. Currently, targeting liver cancer stem cells has become a research hotspot and a new direction for the treatment of HCC. Therefore, further exploring the regulatory mechanisms of liver cancer stem cells and elucidating the pathological mechanisms of HCC hold great clinical significance.

In tumor cells, some key nodal molecules regulate multiple tumor-related signaling pathways. The tyrosine phosphorylation and dephosphorylation states of certain nodal molecules are crucial in the regulation of tumor signaling networks, which are precisely controlled by protein tyrosine kinases and tyrosine phosphatases [11]. Abnormal expression and activation of protein tyrosine kinases have been found in many cancers and play a pivotal role in tumor progression [12]. Proline-rich tyrosine kinase 2 (Pyk2) is a 1995-discovered tyrosine kinase that transduces extracellular signals into the cell via calcium/PKC-dependent phosphorylation of SH2-containing substrates and autophosphorylation, thereby regulating cell adhesion, migration, survival, and proliferation [13, 14]. We have previously reported that higher Pyk2 level in tumor and peritumor tissues was associated with poor outcomes in HCC patients, and that Pyk2 overexpression promoted the proliferation, differentiation and migration of HCC cells through PI3K-AKT pathway [15]. A recent study also highlighted that hypoxia-induced activation of the Pyk2/ERK1/2 pathway in HCC cells promoted HCC progression [16]. Interestingly, miR-23b has been consistently reported to directly target Pyk2, as demonstrated by luciferase reporter assays in both glioma and hepatocellular carcinoma models. In these studies, downregulation of miR-23b promoted tumor progression, whereas its overexpression inhibited cancer cell migration and invasion by suppressing Pyk2 expression [17, 18]. Moreover, multiple databases-based bioinformatics analysis proposed remarkable interaction between Src and miR-23b-3p in HCC [19]. Therefore, this suggests that Pyk2 may play an important role in the malignant progression of HCC by regulating the miR-23b-related signaling pathway. However, its role in the cancer stem cell properties of HCC cells remains to be further explored.

Based on this, the present study aims to explore the role of Pyk2 and its related upstream and downstream signaling pathways in the malignant function of LCSCs and the progression of liver cancer. We first examined the difference in Pyk2 expression levels between liver cancer cells and LCSCs by enriching LCSCs from two liver cancer cell lines. We then constructed LCSC lines with specific Pyk2 knockdown by transfecting siRNA to detect the effects of Pyk2 levels on LCSC functions. In the Pyk2-knockdown cell lines, we co-transfected miR-23b inhibitors to further explore the regulatory effect of miR-23b on the Pyk2 pathway and LCSC functions. Finally, we established a subcutaneous tumor model in BALB/c nude mice and inoculated HCCLM3-LCSC, HCCLM3-LCSC + miR-23b inhibitor, and HCCLM3-LCSC^{siPyk2} + miR-23b inhibitor cells to verify the impact of Pyk2 expression on liver cancer progression by assessing tumor progression, Pyk2 and Src expression in tumor tissues.

Materials and methods

Cell culture and LCSC enrichment

Two liver cancer cell lines, HepG2 (CL-0103, Pricella Biotechnology, Wuhan, China) and HCCLM3 (iCell-h259, iCell Bioscience, Shanghai, China) were used in this study. All cell lines were validated by STR profiling and tested negative for mycoplasma. Cells were all cultured in a humidified incubator at 37 ℃ and 5% CO_2. HCC cells were cultured until they reached the logarithmic growth phase. The cells were then digested into a single-cell suspension, centrifuged, and the supernatant was discarded. The cells were resuspended in DMEM/F12 medium and counted.

The cells were then seeded in a low-adhesion 6-well plate and cultured in LCSC-specific medium, which contained the following growth factors: 10 ng/mL human hepatocyte growth factor (hHGF), 20 ng/mL basic fibroblast growth factor (hβFGF), and 20 ng/mL human epidermal growth factor (hEGF) (HY-P70627, HY-P70440G, HY-P72982, Merck, New Jersey, USA). The cells were cultured and passaged, and the sixth-generation stem cell spheres were used for subsequent experiments.

Cell transfection

The LCSCs were transfected with Pyk2 siRNA to construct the Pyk2 knockdown stem cell lines, with or without miR-23b-3p mimics and inhibitors. A lentiviral vector expressing si-Pyk2 was constructed by Shanghai Genechem Co., Ltd (NM_173174). The miR-23b-3p mimics (Cat. No. RM2233) and inhibitors (Cat. No. RI1233) were purchased from Guangzhou RiboBio Co., Ltd. (Guangzhou, China). Cell transfection was conducted using Lipofectamine 2000 Transfection Reagent (11668019, Invitrogen, California, USA). Briefly, 20pmol siRNA duplex was added to 50 μL of Opti-mem serum-free culture medium. Then, 1 μL of lipo2000 transfection reagent was added to the 50 μL of Opti-mem serum-free culture medium. Mix diluted oligomers with diluted Lipofectamine™ 2000, gently mix, incubate at room temperature for 20 min. The oligomeric Lipofectamine^{TM}2000 complex was added to each pore containing the cells and the medium. The transfected cells were incubated in a cell culture incubator for 24 h before further analysis. Furthermore, the stem cells were also transfected with miR-23b-3p mimics and inhibitors to interfere with the expression of miR-23b-3p. The transcription procedures were also conducted based on the manufacture protocol as above described. The siRNA, miR-23b-3p mimics, and miR-23b-3p inhibitors sequences are shown in Supplement Table 1.

Tumor sphere formation assay

The tumor sphere formation assay was performed to evaluate the stemness of LCSCs using low-attachment 96-well or 6-well plates. Cells were seeded at a density of 2000 cells/mL in the 96-well or 6-well plates. The culture medium was replaced every 2 days. After 10–14 days of culture, the size and number of suspended cell spheres were observed under an inverted microscope.

Colony formation assay

The colony formation assay was performed to evaluate the proliferative capacity of LCSCs. Cells in the logarithmic growth phase were seeded at a density of 1500 cells per well in 6-well plates. The cells were cultured in the incubator for approximately 14 days, with the culture medium replaced every 3–4 days during this period. After the incubation, the 6-well plates were removed, the culture medium was aspirated, and the cells were washed twice with PBS. The cells were then fixed with 4% paraformaldehyde for 20 min. The paraformaldehyde was removed, and the cells were stained with crystal violet solution for 10 min. The crystal violet solution was removed, and the cells were washed with PBS until the rinse was clear. The plates were then air-dried, and images were captured using a camera. The number of cell colonies was quantified.

Wound healing assay

The scratch wound healing assay was performed to assess the migratory capacity of LCSCs. On the back of a 6-well plate, parallel lines were drawn at 0.5 cm intervals, forming a grid pattern. Cells in the logarithmic growth phase were collected, counted, and resuspended at a concentration of 1×10^6 cells/well in the 6-well plate. When the cells reached approximately 90% confluence, a scratch was made perpendicular to the lines on the back of the plate using the tip of a pipette. The cells were then washed twice with PBS, and the initial scratch width was imaged under a microscope. After a designated incubation period, the cells were imaged again under the microscope, and the width of the scratch was recorded. The change in scratch width over time was used to evaluate the cell migration ability.

Transwell assay

The Transwell assay was performed to assess the invasive capacity of LCSCs. The Transwell assay was performed to assess the invasive capacity of LCSCs. Matrigel was diluted with serum-free culture medium and added to the Transwell chamber, which was then incubated at 37 °C for 1 h to solidify. Exponentially growing cells were resuspended in serum-free medium at a density of 1×10^5 cells/mL, and 100 μL of the cell suspension was added to the upper chamber. The lower chamber contained culture medium supplemented with 10% FBS. After 24 h of incubation at 37 °C, the upper chamber was examined, the medium in the lower chamber was replaced with PBS, and the chambers were washed. The cells in the lower chamber were then fixed with 4% paraformaldehyde, stained with crystal violet, and the invaded cells were observed and counted under a microscope.

Flow cytometry

The cell phenotype was determined using flow cytometry. The cells were cultured in a 37 °C, 5% CO_2 incubator for 24 h. The culture medium was then removed from a 6-well plate, and the cells were washed once with 2 mL of PBS. Fresh serum-free medium was added, and the cells were gently pipetted to detach them, with the cell suspension collected. The cell suspension was centrifuged

at 5,000 rpm for 5 min, the supernatant was discarded, and the cells were resuspended in 500 μL of PBS. The cells were counted, and the cell suspension was diluted to 1×10^6 cells/mL. A 50 μL aliquot of the cell suspension (1×10^6 cells/mL) was used for staining, with 10 μL of fluorescently-labeled CD133 (human, FC/FITC, 11-1339-41, Thermo, Massachusetts, USA) and EPCAM (human, FC, 17-0247-41, Thermo, Massachusetts, USA) antibodies added. The cells were incubated with the antibodies at room temperature and in the dark for 60 min. After the incubation, 200 μL of PBS was added, and the cells were centrifuged at 800 rpm for 5 min, with the supernatant discarded. The cells were then washed twice with 2 mL of PBS and resuspended in 300 μL of PBS before being analyzed using a flow cytometer.

CCK-8 assay

Cells were seeded in a 96-well plate at a density of 1×10^4 cells per well, allowed to adhere, and then starved in serum-free medium with 1% BSA for 12 h. The cells were then treated with the test compound or solvent control for the desired duration, followed by the addition of CCK-8 solution (C0038, Beyotime, Shanghai, China). After incubation, the absorbance at 450 nm was measured, and cell viability was calculated using the control group and blank wells as references.

Animal experiments

A subcutaneous tumor xenograft model was established in BALB/c nude mice. The study was conducted in strict adherence to the guidelines for the ethical treatment and welfare of animals. Our animal experimental protocol has been reviewed and approved by the Institutional Animal Care and Use Committee (IACUC) (Approval Number: BSMS2024-02-23B). Briefly, HCCLM3, HCCLM3-LCSC, HCCLM3-LCSC^{siPyk2}, HCCLM3-LCSC + miR-23b inhibitor, and HCCLM3-LCSC^{siPyk2} + miR-23b inhibitor cells were harvested, resuspended in PBS at a concentration of 1×10^7 cells/mL, and subcutaneously inoculated into the dorsal flank of BALB/c nude mice ($n = 30$, 6–8 weeks).

Starting from day 4 after cell inoculation, the length (L, mm) and width (W, mm) of the tumors were measured every 3 days using a vernier caliper. Tumor volume was calculated using the formula: tumor volume = π/6 × L × W2. Tumor growth curves were then plotted. At the end of the experiment, the mice were euthanized, and the tumors were surgically resected, photographed, weighed, and the tumor index was calculated. The tumor index was defined as the ratio of tumor weight (g) to body weight (g). The tumor tissues were used for further immunohistochemical staining.

Immunohistochemical staining

After deparaffinization and rehydration of the paraffin-embedded tissue sections, antigen retrieval was performed by heating the sections in a citrate buffer (pH 6.0) using a microwave oven. A hydrophobic pen was used to draw a circle around the tissue sections, and endogenous peroxidase activity was blocked, followed by overnight incubation with the primary antibody against Pyk2 (dilution 1:100, 17592-1-AP, Proteintech, Wuhan, China) and Src (dilution 1:50, #2105, Cell signaling technology, Massachusetts, USA) at 4 °C. The IHC staining was performed using IHC kits (P0615, Beyotime, Shanghai, China). In brief, after incubation of the primary bodies, the sections were incubated with the Biotin-highly labeled Goat Anti-Rabbit IgG in room temperature for 40 min, and then developed with a Streptavidin (100X) + Biotin-HRP (100X). Lastly, the DAB Horseradish Peroxidase Color Development Kit (P0203, Beyotime, Shanghai, China) was used to stain the sections. The sections were then dehydrated, cleared, mounted with a neutral mounting medium, and observed under microscope.

Real-time quantitative polymerase chain reaction (RT-qPCR) assay

Total RNA was extracted from the cell samples using RNAeasy™ RNA extraction kit (R0027, Beyotime, Shanghai, China) according to the manufacturer's instructions. The concentration and purity of the extracted RNA were measured using a NanoDrop spectrophotometer. Complementary DNA (cDNA) was synthesized from 1 μg of total RNA using a reverse transcription kit (D7168L, Beyotime, Shanghai, China). The RT-qPCR reactions were prepared using a SYBR®Premix Ex TaqTM (Tli RNaseH Plus) (DRR420A, Takara, Liaoning, China). The RT-qPCR reactions were performed on a real-time PCR system with the following cycling conditions: initial denaturation at 95 °C for 10 min, followed by 40 cycles of denaturation at 95 °C for 15 s, annealing and extension at 60 °C for 1 min. Melting curve analysis was conducted to verify the specificity of the amplification. The relative expression levels were calculated using the $2^{-\Delta\Delta Ct}$ method, with GAPDH as the reference gene. The primer sequences are listed in Supplement Table 2.

Protein extraction and Western blot (WB) analysis

The protein expression of Pyk2 and Src were determined using WB assay. Tissue samples were washed 2–3 times with pre-cooled PBS buffer to remove any blood or lipid contaminants, and then cut into small pieces and placed in a homogenizer. 10–20 times the volume of RIPA buffer (P0013B, Beyotime, Shanghai, China) was added, and the samples were thoroughly homogenized on ice. For cell samples, total protein was extracted after trypsin digestion by adding RIPA buffer. The extracted protein

samples were quantified using a BSA protein assay kit, and the samples were diluted accordingly. The diluted samples were then mixed with loading buffer and boiled for 5 min. The protein samples were separated using SDS-PAGE gels with different concentrations, and then transferred to PVDF membranes. The membranes were blocked with milk and incubated with primary antibodies against Pyk2 (dilution 1:1000, 17592-1-AP, Proteintech, Wuhan, China), p-Pyk2 (dilution 1:500, #3291, Cell signaling technology, Massachusetts, USA), Src (dilution 1:1000, #2105, Cell signaling technology, Massachusetts, USA), p-Src (dilution 1:500, #2109, Cell signaling technology, Massachusetts, USA) and GAPDH (dilution 1:10000, ab181602, Abcam, Cambridge, UK) overnight at 4 °C. After washing, the membranes were incubated with the corresponding secondary antibodies HRP-Goat anti Rabbit (dilution 1:10000, AS1107, ASPEN, Wuhan, China). Finally, the protein expression was analyzed using an ECL chemiluminescence detection reagent (AS1059, ASPEN, Wuhan, China) in Chemiluminescence imager. The protein band intensities were quantified using ImageJ software.

Statistical analysis

All experiments were performed in triplicate, and the data are presented as the mean ± standard deviation (SD). Statistical analysis was conducted using GraphPad Prism software (version 8.0). Comparisons between two groups were performed using Student's t-test. For multiple group comparisons, one-way analysis of variance (ANOVA) followed by Tukey's post-hoc test was applied to correct for multiple comparisons. A *P*-value less than 0.05 was considered statistically significant.

Results

Pyk2 expression was significantly elevated in identified LCSCs

Previous studies have suggested that the expression levels of the surface marker proteins CD133 and EPCAM are significantly upregulated in LCSCs [20, 21]. To ensure the enriched HCC was LCSC, we first determined the level of CD133 and EPCAM in these cells. We found that compared to the HepG2 group, the CD133 expression level was significantly higher in the HepG2-LCSC group (Fig. 1A-B, $P<0.001$). Similarly, compared to the HCCLM3 group, the CD133 expression level was significantly higher in the HCCLM3-LCSC group (Fig. 1C-D, $P<0.001$). These results indicate that we successfully isolated liver cancer stem cells.

To investigate whether Pyk2 levels was differentially expressed, we then conducted WB and RT-qPCR assays to further determine the expression levels of Pyk2 in HCC and LCSCs. Further analysis revealed that compared to the HepG2 group, the protein and transcript levels of Pyk2 were significantly upregulated in the HepG2-LCSC group (Fig. 1E, $P<0.05$). Likewise, compared to the HCCLM3 group, the protein and transcript levels of Pyk2 were significantly upregulated in the HCCLM3-LCSC group (Fig. 1F, $P<0.001$). These results suggest that the transcription and expression of Pyk2 are significantly increased in liver cancer stem cells.

Taken together, these findings indicate that Pyk2 may play an important role in the stemness of liver cancer cells.

Construction of Pyk2 knockdown LCSCs

To verify the potential effect of Pyk2 in LCSCs, we constructed Pyk2 knockdown LCSCs by transfecting siRNA to HepG2 and HCCLM3 stem cells. As shown in Fig. 2A-B, we observed that the siRNA-Pyk2-3 exhibited the best interference effect in HepG2-LCSCs, while the siRNA-Pyk2-1 exhibited the best effect in in HCCLM3-LCSCs ($P<0.001$). Hence, siRNA-Pyk2-3 and siRNA-Pyk2-1 were selected for subsequent experiments.

To confirm the effect of si-Pyk2 transfection, we then determined the transcription and protein expression of Pyk2 in HepG2-LCSC^{siPyk2} and HCCLM3-LCSC^{siPyk2}. As expected, we observed that the mRNA level of Pyk2 in both groups were significantly downregulated comparing with HepG2- or HCCLM3-LCSC groups (Fig. 2C-D, $P<0.001$). Also, the protein expression of Pyk2 in HepG2-LCSC^{siPyk2} and HCCLM3-LCSC^{siPyk2} significantly decreased in the Pyk2 knockdown groups (Fig. 2E-F, $P<0.01$ and $P<0.05$).

Therefore, these results suggested that we have successfully constructed the Pyk2 knockdown LCSCs from HepG2 and HCCLM3 cell lines.

Pyk2 expression maintains the stemness of LCSCs

To investigate whether LCSCs stemness was related to the expression of Pyk2, we determined the proliferation, sphere formation, migration, invasion, chemosensitivity, together with the transcriptions of cancer stemness genes including Nanog, Oct4, Sox2, KLF2, Bmil. We found that knockdown of Pyk2 expression significantly suppressed the colony formation and sphere formation abilities of HepG2-LCSCs and HCCLM3-LCSCs (Fig. 3A-D, $P<0.01$). Compared to the HepG2-LCSC^{NC} group, Pyk2 knockdown significantly inhibited the in vitro migration ability of HepG2 stem cells (Fig. 3E, $P<0.001$). Compared to the HCCLM3-LCSC^{NC} group, Pyk2 knockdown significantly suppressed the in vitro migration ability of HCCLM3 stem cells (Fig. 3F, $P<0.001$). Moreover, Pyk2 knockdown significantly inhibited the migration abilities of both types of stem cells (Fig. 3G-H, $P<0.001$).

The transcription levels of stemness genes Nanog, Oct4, Sox2, KLF4, and Bmi1 were all significantly decreased in the HepG2-LCSC^{siPyk2} and HCCLM3-LCSC^{siPyk2} group

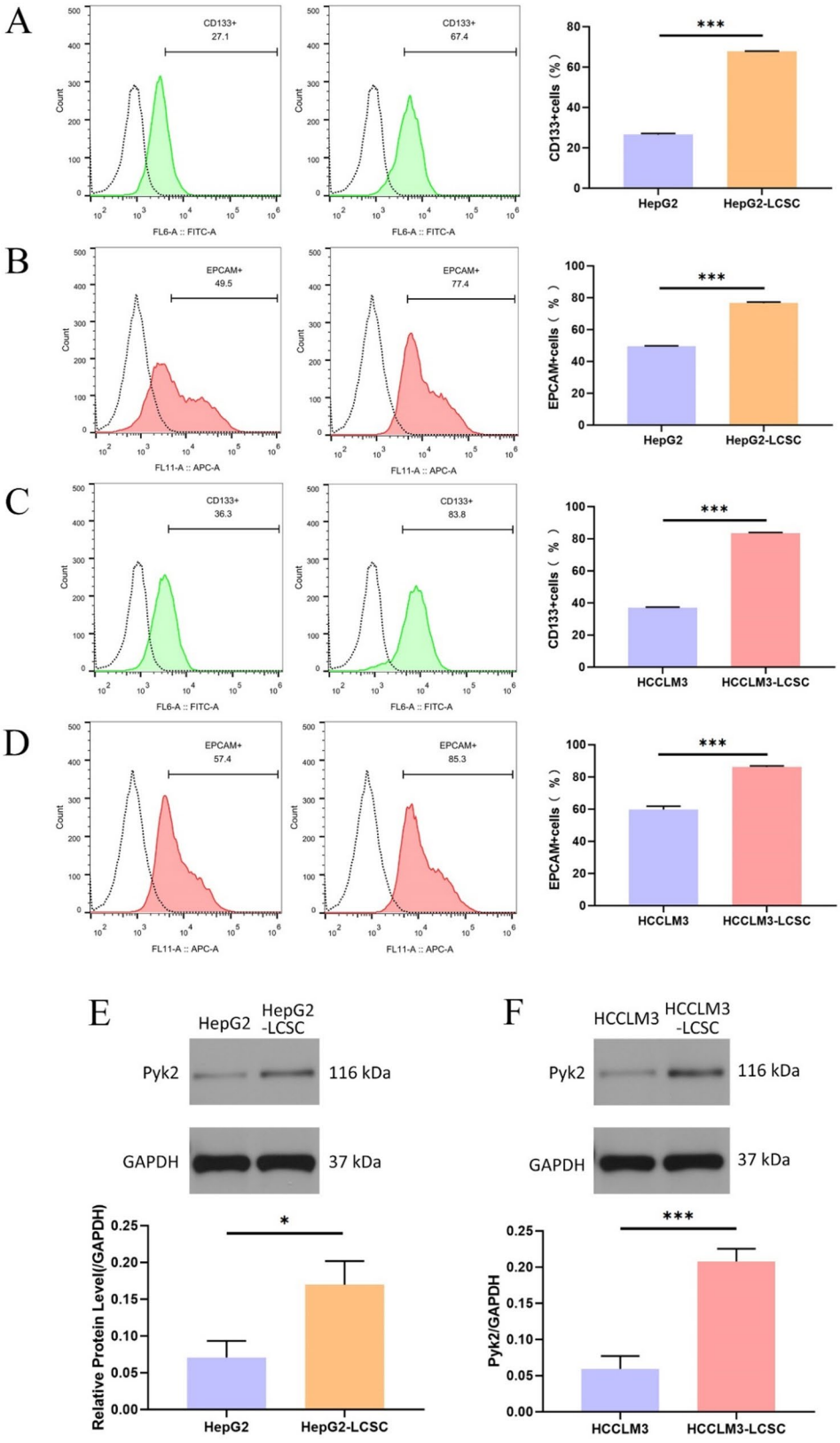

Fig. 1 Pyk2 expression was significantly elevated in identified LCSCs. **(A-B)** The surface marker proteins CD133 and EPCAM of HepG2 and HepG2-LCSCs were measured by flow cytometry. **(C-D)** The surface marker proteins CD133 and EPCAM of HCCLM3 and HCCLM3-LCSCs were measured by flow cytometry. **(E-F)** The expression of Pyk2 in HepG2, HCCLM3, and relative LCSCs were measured using WB. Data are presented as mean ± standard deviation; $^{*}P < 0.05$, $^{**}P < 0.01$, $^{***}P < 0.001$; $n = 3$

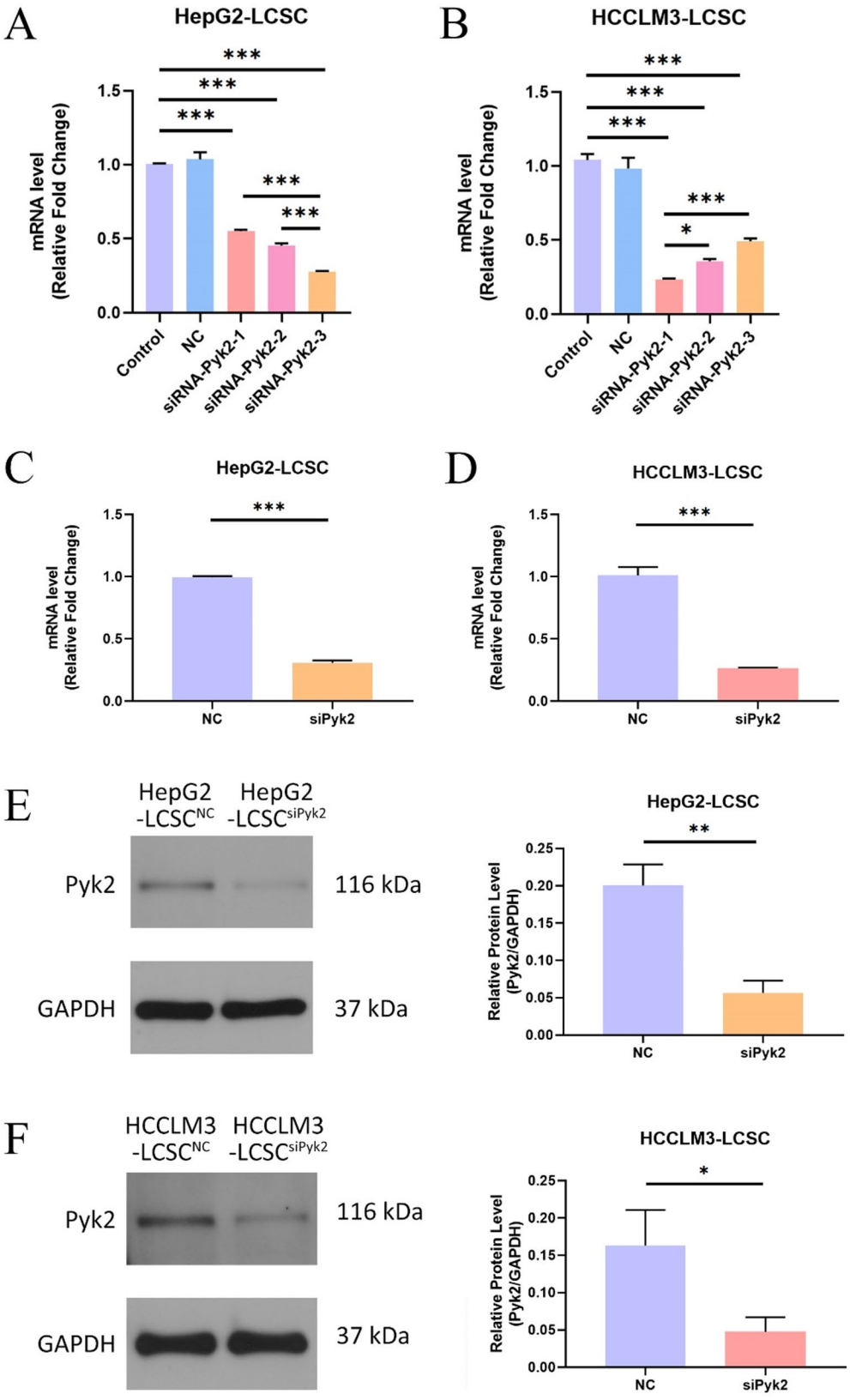

Fig. 2 Construction of Pyk2 knockdown LCSCs. **(A-B)** The Pyk2 knockdown LCSCs were constructed by siRNA transfection. **(C-D)** The mRNA levels of Pyk2 in HepG2-LCSCs^{siPyk2} and HCCLM3-LCSCs ^{siPyk2} were determined by RT-qPCR. **(E-F)** The protein expressions of Pyk2 in HepG2-LCSCs^{siPyk2} and HCCLM3-LCSCs ^{siPyk2}s were determined by WB. Data are presented as mean ± standard deviation; $^{*}P < 0.05$, $^{**}P < 0.01$, $^{***}P < 0.001$; $n = 3$

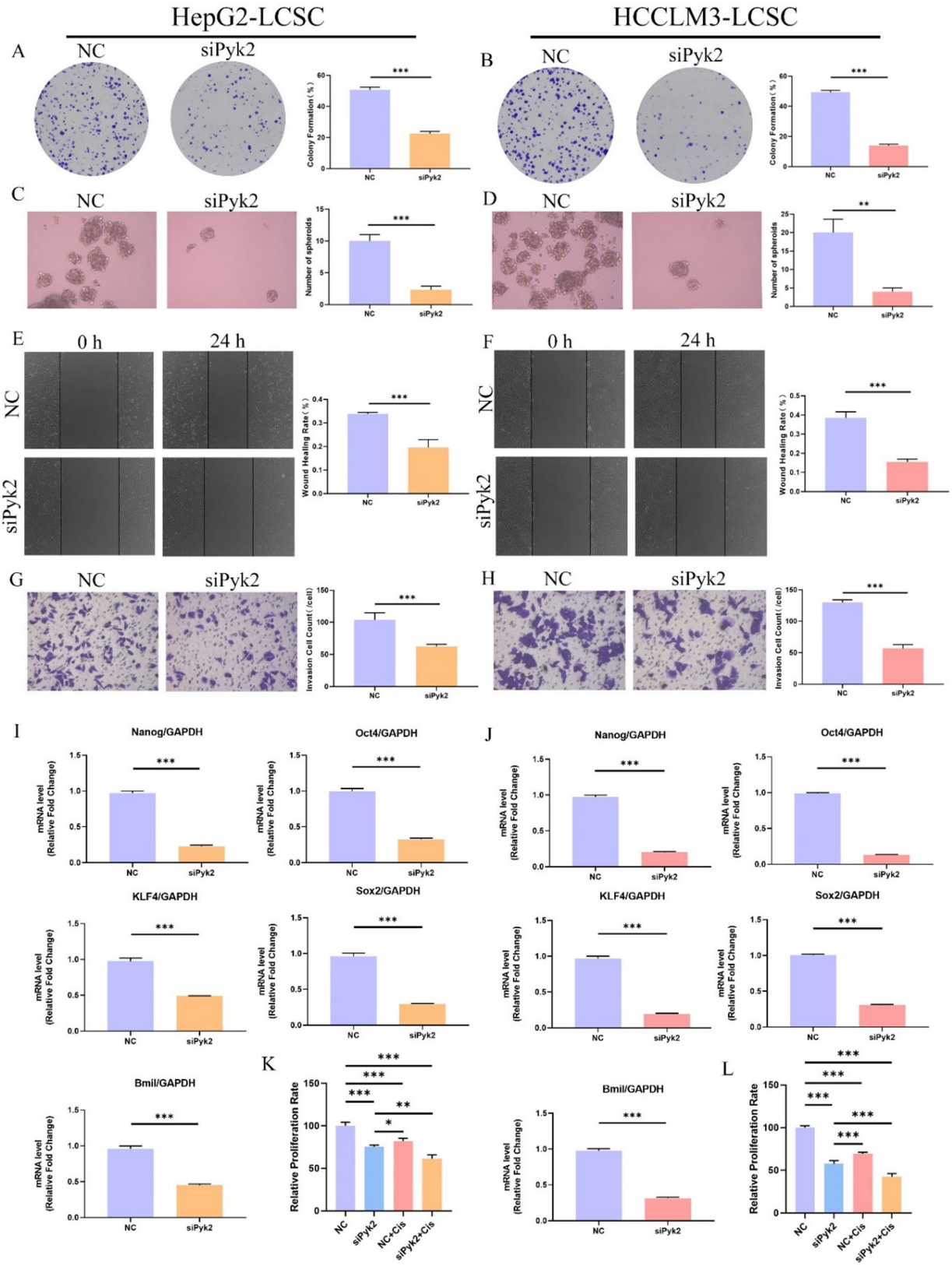

Fig. 3 (See legend on next page.)

(See figure on previous page.)

Fig. 3 Pyk2 expression maintain the stemness of LCSCs. **(A-B)** Colony formation assays of HepG2-LCSCs **(A)** and HCCLM3-LCSCs **(B)** transfected with Pyk2 siRNA (siPyk2) or negative control (NC). **(C-D)** Tumorsphere formation assays in the same groups as above for HepG2-LCSCs **(C)** and HCCLM3-LCSCs **(D)**. **(E-F)** Wound healing assays showing migratory capacity at 0 h and 24 h in HepG2-LCSCs **(E)** and HCCLM3-LCSCs **(F)** after Pyk2 knockdown. **(G-H)** Transwell invasion assays evaluating invasive ability of HepG2-LCSCs **(G)** and HCCLM3-LCSCs **(H)** under Pyk2 knockdown versus control conditions. **(I-J)** RT-qPCR analysis of stemness-related gene expression (Nanog, Oct4, Sox2, KLF4, Bmi1) in HepG2-LCSCs **(I)** and HCCLM3-LCSCs **(J)** following siPyk2 or NC treatment. **(K-L)** Cell proliferation and cisplatin sensitivity assessed by CCK-8 assay in HepG2-LCSCs **(K)** and HCCLM3-LCSCs **(L)**, respectively. Data are presented as mean ± standard deviation; *$P<0.05$, **$P<0.01$, ***$P<0.001$; $n=3$

(Fig. 3I-J, $P<0.001$). Importantly, we observed that Pyk2 knockdown had the property to inhibit the proliferation of HepG2 and HCCLM3 stem cells (Fig. 3K-L, $P<0.001$). When treated with cisplatin, the proliferation of HepG2 and HCCLM3 stem cells were further inhibited in Pyk2 knockdown groups comparing with NC + Cis groups (Fig. 3K-L, $P<0.01$).

Therefore, these results indicated that inhibiting Pyk2 expression reduced the proliferation, sphere formation, migration, invasion, and increased chemosensitivity of LCSCs, which further suggested that Pyk2 expression promoted the stemness of LCSCs.

miR-23b-3p inhibits Pyk2/Src signaling in LCSCs

Previous study pointed out that miR-23b-3p inhibition was closely related to HCC progression, which was predicted to interact with Src using protein-protein network enrichment. Therefore, we aimed to further explore the potential upstream and downstream signaling of Pyk2 expression.

To determine whether Pyk2 is a direct target of miR-23b-3p, a dual-luciferase reporter assay was performed. As shown in Fig. 4A, co-transfection of miR-23b-3p mimics significantly reduced the luciferase activity of the wild-type Pyk2 3'-UTR reporter, but not that of the mutant construct, indicating direct binding of miR-23b-3p to the Pyk2 3'-UTR (Fig. 4A, $P<0.001$). Conversely, inhibition of miR-23b-3p increased luciferase activity in the wild-type construct, further supporting this interaction (Fig. 4A, $P<0.05$). These results indicate that miR-23b-3p is a negative regulator of Pyk2 gene expression.

Next, we analyzed endogenous miR-23b-3p expression in different liver cancer cell models. As shown in Fig. 4B, the expression level of miR-23b-3p was significantly reduced in HCCLM3 cells compared to HepG2 cells ($P<0.001$), and further downregulated in HCCLM3-derived LCSCs ($P<0.001$), suggesting a potential link between miR-23b-3p downregulation and stem-like malignancy in hepatocellular carcinoma. It is worth noting that Pyk2 expression was significantly upregulated in HCCLM3-LCSCs treated with miR-23b-3p inhibitor (Fig. 4C, $P<0.001$), which further proved that miR-23b-3p downregulated Pyk2 expression in LCSCs. As shown in Fig. 4D-I, in Pyk2 knockdown HCCLM3-LCSCs, the relative expression of p-Pyk2/Pyk2 and p-Src/Src were significantly decreased comparing to the HCCLM3-LCSC group ($P<0.001$). When Pyk2 knockdown HCCLM3-LCSCs was treated with miR-23b-3p inhibitor, the inhibitory effect on these proteins by Pyk2 silencing was abolished.

These results suggest that the inhibition of miR-23b-3p can restore the expression of the Pyk2 signaling pathway (p-Pyk2/Pyk2 and p-Src/Src) in HCCLM3-LCSCs with Pyk2 knockdown, effectively reversing the suppressive effects caused by Pyk2 silencing. This indicates that miR-23b-3p may be an important regulator of the Pyk2/Src signaling axis in HCCLM3-LCSCs.

miR-23b-3p down-regulates Pyk2 expression to reduce the proliferation, migration, invasion, and chemosensitivity of LCSCs

We then observed the effect of miR-23b-3p mediated Pyk2 signaling on the malignancy of LCSCs. Comparing with control, miR-23b-3p inhibitor significantly facilitated the proliferation, migration, and invasion of HCCLM3-LCSCs (Fig. 5A, C, E, $P<0.001$). Also, the chemosensitivity of miR-23b-3p inhibited HCCLM3-LCSCs was decreased (Fig. 5E, $P<0.001$). Compared with HCCLM3-LCSC group, the transcription levels of stemness genes Nanog, Oct4, Sox2, KLF4 and Bmil were significantly increased after treatment with miR-23b-3p inhibitor in HCCLM3-LCSCs (Fig. 5G, $P<0.001$).

On the other hand, the proliferation, migration, and invasion were inhibited in Pyk2 knockdown HCCLM3-LCSCs, whereas the chemosensitivity was largely improved comparing with HCCLM3-LCSCs (Fig. 5B, D, F, $P<0.001$). Likewise, the transcription levels of Nanog, Oct4, Sox2, KLF4 and Bmil genes were pronouncedly downregulated in HCCLM3-LCSC^{siPyk2} group (Fig. 5H, $P<0.05$). However, these positive effects induced by Pyk2 inhibition were abrogated when HCCLM3 stem cells were further knockdown in the presence of miR-23b-3p inhibitor. The proliferation, migration, and invasion of miR-23b-3p inhibited HCCLM3-LCSC^{siPyk2} were similar to those in the HCCLM3-LCSC group (Fig. 5B, D, F, $P>0.05$). And the mRNA levels of Bmil was also similar to control ($P<0.05$), whereas the levels of Nanog, Oct4, and SOX2 were even upregulated in miR-23b-3p inhibited HCCLM3-LCSC^{siPyk2} group at different levels (Fig. 5H, $P<0.05$).

These results suggest that the inhibition of miR-23b-3p can reverse the suppressive effects on HCCLM3-LCSC malignancy and stemness induced by Pyk2 knockdown,

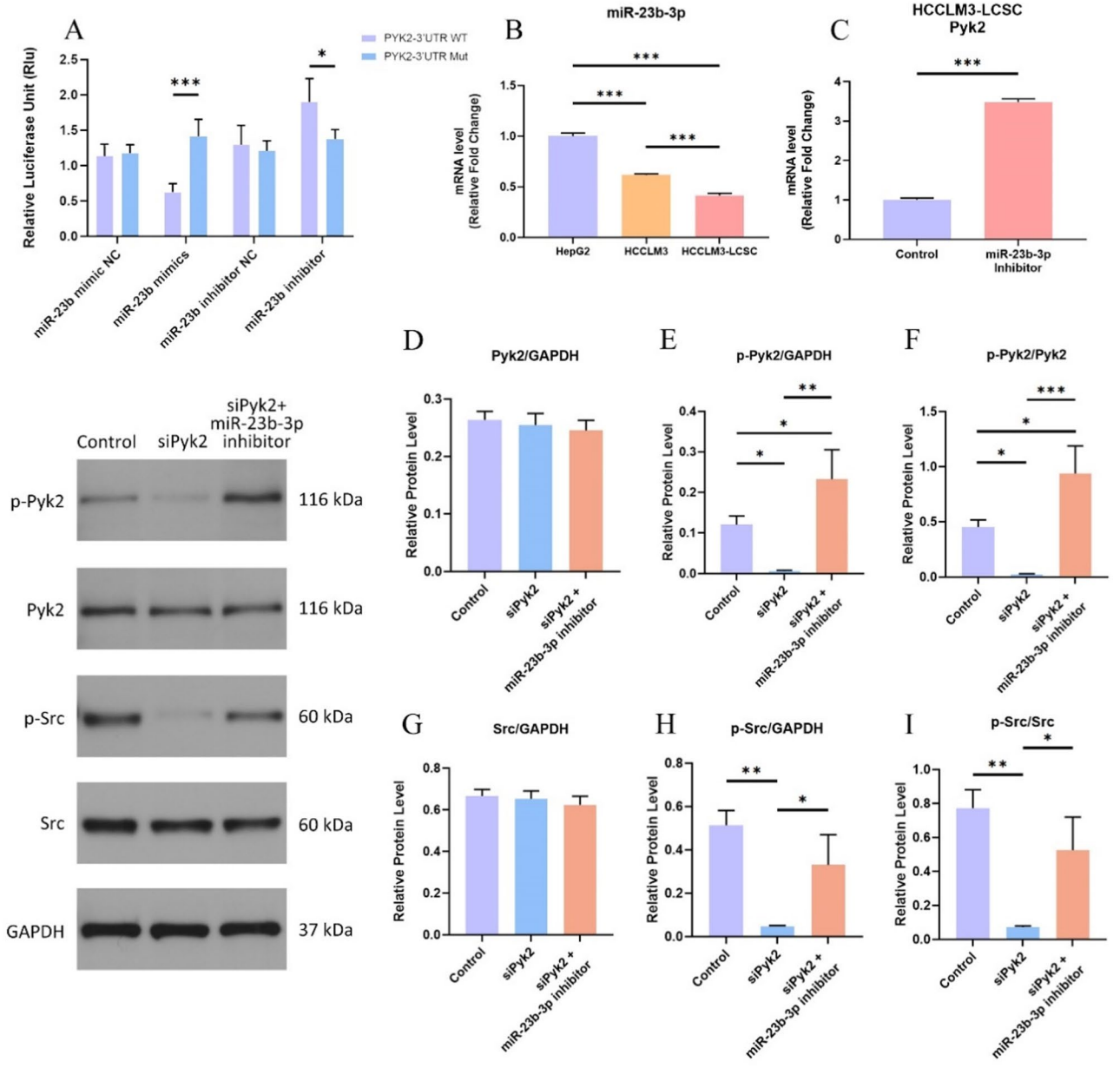

Fig. 4 miR-23b-3p inhibits Pyk2/Src signaling in LCSCs. **(A)** Dual-luciferase reporter assay in HCCLM3-LCSCs co-transfected with wild-type or mutant Pyk2 3′-UTR constructs and miR-23b-3p mimic or inhibitor, demonstrating direct binding between miR-23b-3p and the Pyk2 3′-UTR. **(B)** RT-qPCR quantification of endogenous miR-23b-3p expression in HepG2, HCCLM3, and HCCLM3-LCSC cells. **(C)** Pyk2 mRNA levels measured by RT-qPCR in HCCLM3-LCSCs after transfection with miR-23b-3p inhibitor. **(D-F)** Western blot and quantitative analysis of total Pyk2 **(D)**, phosphorylated Pyk2 **(E)**, and p-Pyk2/Pyk2 ratio **(F)** in HCCLM3-LCSCs transfected with siPyk2, or co-transfected with siPyk2 and miR-23b-3p inhibitor. **(G-I)** Western blot and quantification of total Src **(G)**, phosphorylated Src **(H)**, and p-Src/Src ratio **(I)** in the same treatment groups. Data are presented as mean ± standard deviation; *$P < 0.05$, **$P < 0.01$, ***$P < 0.001$; $n = 3$

indicating that miR-23b-3p acts as an important regulator of the Pyk2 signaling pathway in controlling LCSC properties.

miR-23b promotes HCC progression by regulating Pyk2/Src expression in balb/c mice

The in vivo xenograft experiment showed that the tumor volume and weight were significantly smaller in the HCCLM3 group compared to the HCCLM3-LCSC group. The HCCLM3-LCSCsiPyk2 group exhibited reduced tumor growth compared to the HCCLM3-LCSC group, but the tumor size was still larger than that of the HCCLM3 group (Fig. 6A-C, $P < 0.001$). Interestingly, the HCCLM3-LCSCsiPyk2 group co-treated with the miR-23b inhibitor had tumor sizes similar to the HCCLM3-LCSC group with the miR-23b inhibitor (Fig. 6A-C,

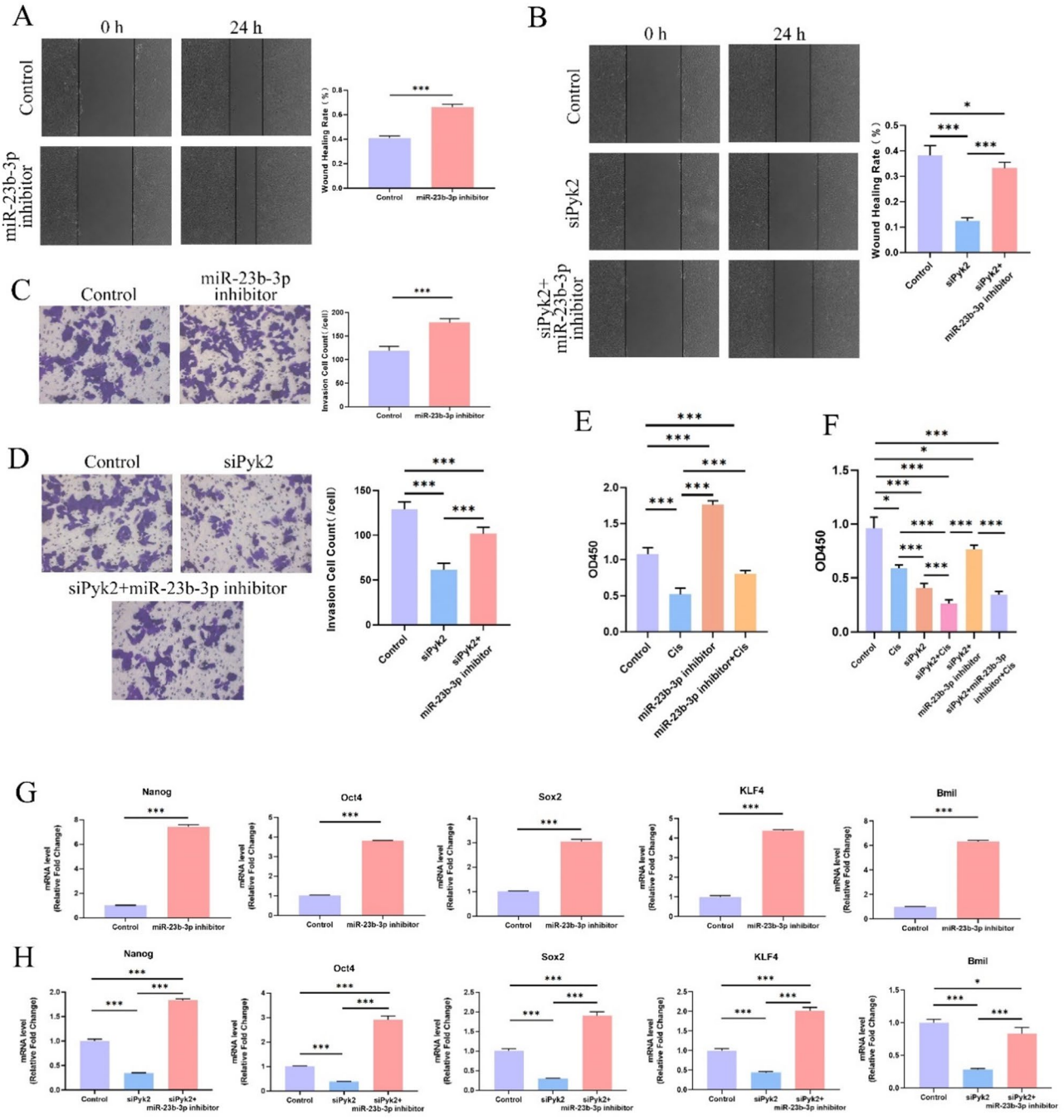

Fig. 5 miR-23b-3p down-regulates Pyk2 expression to reduce the proliferation, migration, invasion, and chemosensitivity of LCSCs. **(A-B)** Wound healing assays evaluating the migration rate of HCCLM3-LCSCs transfected with miR-23b-3p inhibitor **(A)**, as well as siPyk2 and/or miR-23b-3p inhibitor **(B)**. **(C-D)** Transwell invasion assays assessing invasive ability of the same treatment groups as in **(A-B)**, showing increased invasion upon miR-23b-3p inhibition and partial rescue by siPyk2. **(E-F)** CCK-8 assays quantifying proliferation **(E)** and cisplatin-induced chemosensitivity **(F)** in HCCLM3-LCSCs after miR-23b-3p inhibition, with or without Pyk2 knockdown. **(G-H)** RT-qPCR analysis of stemness-related genes (Nanog, Oct4, Sox2, KLF4, Bmi1) in miR-23b-3p-inhibited LCSCs **(G)**, and in control, siPyk2, and siPyk2 + miR-23b-3p inhibitor groups **(H)**. Data are presented as mean ± standard deviation; *$P < 0.05$, **$P < 0.01$, ***$P < 0.001$; $n = 3$

$P < 0.001$), suggesting that the inhibition of miR-23b could partially rescue the effects of Pyk2 silencing.

Furthermore, the expression levels of Pyk2 and Src in the tumor tissues reflected the observed differences in tumor growth. As shown in Fig. 6D-E, the HCCLM3 group had the lowest Pyk2 and Src expression, followed by the HCCLM3-LCSCsiPyk2 group. The HCCLM3-LCSC group and the HCCLM3-LCSCsiPyk2 group with

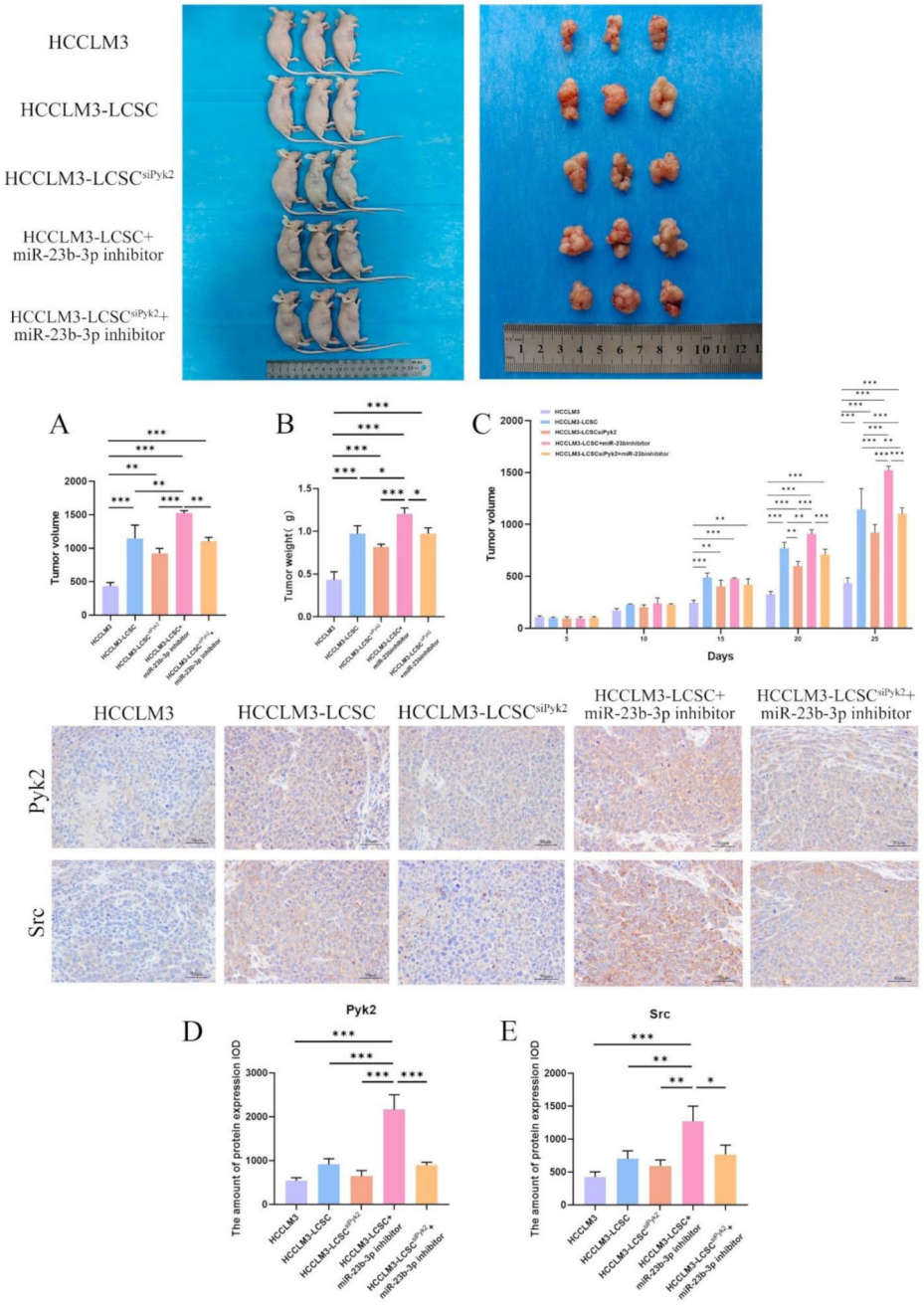

Fig. 6 miR-23b promotes HCC progression by regulating Pyk2/Src expression in BALB/c mice. **(A-C)** HCCLM3 and interfered HCCLM3-LCSCs (control, siPyk2, miR-23b-3p inhibitor, or siPyk2 + miR-23b-3p inhibitor) were subcutaneously injected into BALB/c nude mice ($n = 3$ per group). Tumors were excised at the end of the experiment for volume **(A)** and weight **(B)** assessment, tumor volume was monitored every 3 days **(C)**. **(D-E)** Representative images and quantitative analysis of immunohistochemical staining of Pyk2 and Src in tumor tissues from each group. Scale bar: 50 μm. Data are presented as mean ± standard deviation; $^{*}P < 0.05$, $^{**}P < 0.01$, $^{***}P < 0.001$; $n = 3$

the miR-23b inhibitor had similar Pyk2 and Src expression levels, which were higher than the HCCLM3-LCSC-siPyk2 group but lower than the HCCLM3-LCSC group with the miR-23b inhibitor.

Therefore, our results suggested that miR-23b promotes HCC progression by regulating Pyk2/Src expression in BALB/c mice.

Discussion

Liver cancer is one of the most prevalent and deadly malignancies worldwide, with LCSCs playing a critical role in tumor initiation, progression, metastasis, and recurrence [22, 23]. Identifying key molecular regulators of LCSC stemness properties is essential for developing more effective therapies. Therefore, this study aimed to provide insights into the role of Pyk2 in regulating the stemness of LCSCs, and to develop its underlying mechanisms in regulating the malignancy and stemness of LCSCs. Here, we demonstrated that Pyk2 expression promotes the stemness of LCSCs, and inhibition of Pyk2 can effectively suppress LCSC malignancy. Furthermore, we show that miR-23b-3p acts as a critical regulator of the Pyk2/Src signaling axis in controlling LCSC properties.

Pyk2 is a non-receptor tyrosine kinase that has been implicated in the regulation of various cellular processes, including cell migration, invasion, and survival [24]. As previously reported, Pyk2 is a critical component of the focal adhesion signaling pathway, activation of Pyk2 leads to enhanced cytoskeletal remodeling, transendothelial migration of monocytes/macrophages, and subsequent M2 polarization, thereby facilitating tumor progression and metastasis in colorectal cancer [25]. Our findings demonstrate that Pyk2 expression is important for the stemness properties of LCSCs. Specifically, knockdown of Pyk2 in HepG2 and HCCLM3 LCSCs led to reduced proliferation, sphere formation, migration, and invasion, and increased chemosensitivity. These results suggest that Pyk2 expression promotes the stemness of LCSCs, and inhibition of Pyk2 can effectively suppress LCSC malignancy.

MicroRNAs are known to play crucial roles in regulating cancer stem cell properties. A growing number of studies have proven that miR-23b act as tumor suppressor to inhibit the EMT, proliferation, migration, and invasion of HCC [26–29]. On the other hand, a study has also reported an oncogenic role of miR-23b-3p in HCC. Hayashi et al. demonstrated that miR-23b-3p functions as an oncogenic microRNA that promotes cancer progression by enhancing cell proliferation in SK-Hep1 cells, while its inhibition suppressed proliferation in HepG2 cells [30]. In their clinical cohort of 125 resected HCC patients, miR-23b-3p expression was elevated in 38% of tumors and downregulated in the remaining 62%, reflecting a heterogeneous expression pattern across patients. Although elevated miR-23b-3p levels were associated with worse recurrence-free and overall survival, the study did not perform multivariate analysis to account for potential confounding clinical variables such as tumor stage, vascular invasion, or liver function. A study by Sun et al. evaluated serum miR-23b-3p in patients with early-stage HCV-related HCC and reported that its level was significantly reduced in the serum of HCC patients compared to chronic liver disease and healthy controls [31]. Interestingly, miR-23b-3p levels increased significantly after surgical resection, highlighting the complexity of interpreting miR-23b-3p levels in different biological compartments (tissue vs. circulation) and disease stages. Further investigations on the role of miR-23b-3p is in needed to clarify the controversy function of miR-23b-3p, especially in HCC. Here, we observed that miR-23b-3p level in the HCCLM3 stem cells displayed remarkable reduction comparing with HCCLM3 cells, while did not show significant differences in HepG2-LCSCs. Since HCCLM3 is reported to be the highly metastatic human liver cancer cell line [32], these results indicated that miR-23b-3p might be crucial in the malignancy of HCC, especially in LCSCs. Our results supported the theory that miR-23b-3p acts as a tumor suppressing gene.

Notably, Pyk2 has already been validated as a direct target of miR-23b by luciferase reporter assays in multiple contexts. Loftus et al. demonstrated that miR-23b suppresses glioblastoma cell migration and invasion by targeting the 3'-UTR of Pyk2 [17]. We have also reported that miR-23b inhibits EMT and metastasis in HCC by directly binding to the Pyk2 3'-UTR, as confirmed through luciferase reporter analysis in previously published study [18]. Moreover, Pyk2 promotes cancer progression in part by interacting with and activating c-Src. This activation leads to recruitment of the Grb2/SOS complex and stimulation of the ERK1/2 pathway, thereby enhancing cell proliferation and survival through regulation of apoptosis-related proteins [33]. Here, we observed that the inhibition of miR-23b-3p in Pyk2 knockdown HCCLM3-LCSCs was able to restore the expression of the Pyk2/Src signaling pathway, and reverse the suppressive effects caused by Pyk2 silencing. This indicates that miR-23b-3p is an important regulator of the Pyk2/Src axis in controlling LCSC malignancy and stemness. Further experiments demonstrated that the inhibition of miR-23b-3p could effectively reverse the Pyk2 knockdown-induced suppression of HCCLM3-LCSC proliferation, sphere formation, migration, and invasion. These results suggest that miR-23b-3p acts as a critical regulator of the Pyk2 signaling pathway in LCSCs, and targeting the miR-23b-3p/Pyk2/Src axis may be a promising strategy for LCSC-directed therapy.

While this study provides valuable insights into the regulatory mechanisms governing LCSC stemness, there

are several limitations that should be addressed in future research. First, the in vivo experiments were conducted using a mouse xenograft model, which may not fully recapitulate the complex tumor microenvironment in human patients. Additional studies using patient-derived xenograft models or transgenic mouse models would be helpful to further validate the clinical relevance of our findings. Second, the specific mechanisms by which miR-23b-3p regulates the Pyk2/Src signaling pathway require further investigation. Exploring the upstream regulators and downstream effectors of this axis may yield important insights into the signaling networks controlling LCSC properties. Third, although our results suggest that miR-23b-3p negatively regulates Pyk2, further experimental confirmation in LCSCs or animal models specifically would strengthen the mechanistic conclusions. Finally, although our findings highlight the miR-23b-3p/Pyk2/Src axis as a critical pathway driving liver cancer stemness and malignancy, there are currently no clinically available therapies that directly target this regulatory axis. This underscores an important need in HCC treatment, particularly for patients with aggressive tumor subtypes. Future research should focus on the development and validation of therapeutic strategies that modulate miR-23b-3p activity, either through the restoration of its expression or the application of synthetic miRNA mimics. Given the well-established role of Pyk2/Src signaling in tumor invasion, proliferation, and drug resistance, targeting this pathway via miR-23b-3p modulation may represent a promising therapeutic strategy. In particular, the restoration of miR-23b-3p expression could be explored as a means to disrupt this oncogenic signaling cascade in aggressive HCC subtypes. However, further studies are needed to assess the efficacy, delivery methods, and safety profiles of such approaches in preclinical and clinical settings.

Conclusion

In conclusion, our study has uncovered a critical role for the Pyk2/Src signaling pathway in regulating the stemness of LCSCs, and has identified miR-23b-3p as a key upstream regulator of this axis. These findings suggest that targeting the miR-23b-3p/Pyk2/Src signaling axis may be a promising approach for LCSC-directed therapy in liver cancer.

Supplementary Information

The online version contains supplementary material available at https://doi.org/10.1186/s12935-025-03841-8.

Supplementary Material 1

Acknowledgements
The authors would like to express their gratitude to all the participants and staff who were involved in this study.

Author contributions
Meng Sha, Jiang Zhang: Methodology, Investigation, Formal analysis, Writing - original draft, Conceptualization; Jin-kai Liu, Xiao-ye Qu, Chuan Shen, Ying Tong: Methodology, Investigation, Formal analysis, Visualization, Data Curation, Software; Jie Cao: Writing - review & editing, Project administration, Methodology, Investigation, Supervision, Resources, Conceptualization.

Funding
The authors declare that no funds, grants, or other support were received during the preparation of this manuscript.

Data availability
The datasets used and/or analyzed during the current study are available from the corresponding author on reasonable request.

Declarations

Ethics approval and consent to participate
Animal feeding and experimental operations were performed at the Experimental Animal Center of Renji Hospital, School of Medicine, Shanghai Jiao Tong University. The treatment of experimental animals strictly followed the principles of "reduction, substitution, and optimization" and was provided humanely. The experimental protocol has been reviewed and approved by the Institutional Animal Care and Use Committee (IACUC), Number: BSMS2024-02-23B.

Consent for publication
Not applicable.

Competing interests
The authors declare no competing interests.

Clinical trial number
Not applicable.

Received: 6 March 2025 / Accepted: 31 May 2025
Published online: 07 June 2025

References

1. Ganesan P, Kulik LM. Hepatocellular carcinoma. Clin Liver Dis. 2023;27:85–102. https://doi.org/10.1016/j.cld.2022.08.004.
2. Alawyia B, Constantinou C. Hepatocellular carcinoma: a narrative review on current knowledge and future prospects. Curr Treat Options Oncol. 2023;24:711–24. https://doi.org/10.1007/s11864-023-01098-9.
3. Galle PR, Dufour J-F, Peck-Radosavljevic M, Trojan J, Vogel A. Systemic therapy of advanced hepatocellular carcinoma. Future Oncol. 2020;17:1237–51. https://doi.org/10.2217/fon-2020-0758.
4. Sugawara Y, Hibi T. Surgical treatment of hepatocellular carcinoma. Biosci Trends. 2021;15:138–41. https://doi.org/10.5582/bst.2021.01094.
5. Niu Q, Ye S, Zhao L, Qian Y, Liu F. The role of liver cancer stem cells in hepatocellular carcinoma metastasis. Cancer Biol Ther. 2024;25. https://doi.org/10.1080/15384047.2024.2321768.
6. Walcher L, Kistenmacher A-K, Suo H, Kitte R, Dluczek S, Strauß A, et al. Cancer stem Cells—Origins and biomarkers: perspectives for targeted personalized therapies. Front Immunol. 2020;11. https://doi.org/10.3389/fimmu.2020.01280.
7. Biserova K, Jakovlevs A, Uljanovs R, Strumfa I. Cancer stem cells: significance in origin, pathogenesis and treatment of glioblastoma. Cells. 2021;10. https://doi.org/10.3390/cells10030621.
8. Butti R, Gunasekaran VP, Kumar TVS, Banerjee P, Kundu GC. Breast cancer stem cells: biology and therapeutic implications. Int J Biochem Cell Biol. 2019;107:38–52. https://doi.org/10.1016/j.biocel.2018.12.001.
9. Liu Y-C, Yeh C-T, Lin K-H. Cancer stem cell functions in hepatocellular carcinoma and comprehensive therapeutic strategies. Cells. 2020;9. https://doi.org/10.3390/cells9061331.
10. Lee TK-W, Guan X-Y, Ma S. Cancer stem cells in hepatocellular carcinoma — from origin to clinical implications. Nat Rev Gastroenterol Hepatol. 2021;19:26–44. https://doi.org/10.1038/s41575-021-00508-3.

11. Yang Y, Li S, Wang Y, Zhao Y, Li Q. Protein tyrosine kinase inhibitor resistance in malignant tumors: molecular mechanisms and future perspective. Signal Transduct Target Ther. 2022;7. https://doi.org/10.1038/s41392-022-01168-8.
12. Taddei ML, Pardella E, Pranzini E, Raugei G, Paoli P. Role of tyrosine phosphorylation in modulating cancer cell metabolism. Biochim Biophys Acta Rev Cancer. 2020;1874. https://doi.org/10.1016/j.bbcan.2020.188442.
13. Gil-Henn H, Girault J-A, Lev S. PYK2, a hub of signaling networks in breast cancer progression. Trends Cell Biol. 2024;34:312–26. https://doi.org/10.1016/j.tcb.2023.07.006.
14. Shen T, Guo Q. Role of Pyk2 in human cancers. Med Sci Monit. 2018;24:8172–82. https://doi.org/10.12659/msm.913479.
15. Cao J, Chen Y, Fu J, Qian Y-W, Ren Y-B, Su B, et al. High expression of Proline-Rich tyrosine Kinase2 is associated with poor survival of hepatocellular carcinoma via regulating phosphatidylinositol 3-Kinase/AKT pathway. Ann Surg Oncol. 2012;20:312–23. https://doi.org/10.1245/s10434-012-2372-9.
16. Chen T, Wang L, Chen C, Li R, Zhu N, Liu R, et al. HIF-1α-activated TMEM237 promotes hepatocellular carcinoma progression via the NPHP1/Pyk2/ERK pathway. Cell Mol Life Sci. 2023;80. https://doi.org/10.1007/s00018-023-04767-y.
17. Loftus JC, Ross JT, Paquette KM, Paulino VM, Nasser S, Yang Z, et al. MiRNA expression profiling in migrating glioblastoma cells: regulation of cell migration and invasion by miR-23b via targeting of Pyk2. PLoS ONE. 2012;7:e39818. https://doi.org/10.1371/journal.pone.0039818.
18. Cao J, Liu J, Long J, Fu J, Huang L, Li J, et al. microRNA-23b suppresses epithelial-mesenchymal transition (EMT) and metastasis in hepatocellular carcinoma via targeting Pyk2. Biomed Pharmacother. 2017;89:642–50. https://doi.org/10.1016/j.biopha.2017.02.030.
19. He R-Q, Wu P-R, Xiang X-L, Yang X, Liang H-W, Qiu X-H, et al. Downregulated miR-23b-3p expression acts as a predictor of hepatocellular carcinoma progression: A study based on public data and RT-qPCR verification. Int J Mol Med. 2018. https://doi.org/10.3892/ijmm.2018.3513.
20. Cheng Q, Ning S, Zhu L, Zhang C, Jiang S, Hao Y, et al. NDRG1 facilitates self-renewal of liver cancer stem cells by preventing EpCAM ubiquitination. Br J Cancer. 2023;129:237–48. https://doi.org/10.1038/s41416-023-02278-y.
21. Wang L, Deng C-H, Luo Q, Su X-B, Shang X-Y, Song S-J, et al. Inhibition of Arid1a increases stem/progenitor cell-like properties of liver cancer. Cancer Lett. 2022;546. https://doi.org/10.1016/j.canlet.2022.215869.
22. Anwanwan D, Singh SK, Singh S, Saikam V, Singh R. Challenges in liver cancer and possible treatment approaches. Biochim Biophys Acta Rev Cancer. 2020;1873. https://doi.org/10.1016/j.bbcan.2019.188314.
23. Cheng K, Cai N, Zhu J, Yang X, Liang H, Zhang W. Tumor-associated macrophages in liver cancer: from mechanisms to therapy. Cancer Commun. 2022;42:1112–40. https://doi.org/10.1002/cac2.12345.
24. Lee D, Hong J-H. Activated PyK2 and its associated molecules transduce cellular signaling from the cancerous milieu for Cancer metastasis. Int J Mol Sci. 2022;23. https://doi.org/10.3390/ijms232415475.
25. Huang C, Ou R, Chen X, Zhang Y, Li J, Liang Y, et al. Tumor cell-derived SPON2 promotes M2-polarized tumor-associated macrophage infiltration and cancer progression by activating PYK2 in CRC. J Exp Clin Cancer Res. 2021;40. https://doi.org/10.1186/s13046-021-02108-0.
26. Park NR, Cha JH, Sung PS, Jang JW, Choi JY, Yoon SK, et al. MiR-23b-3p suppresses epithelial-mesenchymal transition, migration, and invasion of hepatocellular carcinoma cells by targeting c-MET. Heliyon. 2022;8. https://doi.org/10.1016/j.heliyon.2022.e11135.
27. Xiong J, Lai Y, Cheng N, Liu J, Wang F, Zheng X, et al. Lnc-PLA2G4A-4 facilitates the progression of hepatocellular carcinoma by inducing versican expression via sponging miR-23b-3p. Heliyon. 2023;9. https://doi.org/10.1016/j.heliyon.2023.e18698.
28. Kaur R, Kanthaje S, Taneja S, Dhiman RK, Chakraborti A. miR-23b-3p modulating cytoprotective autophagy and glutamine addiction in Sorafenib resistant HepG2, a hepatocellular carcinoma cell line. Genes. 2022;13. https://doi.org/10.3390/genes13081375.
29. Yang X, Yang S, Song J, Yang W, Ji Y, Zhang F, et al. Dysregulation of miR-23b-5p promotes cell proliferation via targeting FOXM1 in hepatocellular carcinoma. Cell Death Discov. 2021;7:47. https://doi.org/10.1038/s41420-021-00440-0.
30. Hayashi M, Yamada S, Kurimoto K, Tanabe H, Hirabayashi S, Sonohara F, et al. miR-23b-3p plays an oncogenic role in hepatocellular carcinoma. Ann Surg Oncol. 2020;28:3416–26. https://doi.org/10.1245/s10434-020-09283-y.
31. Hayashi M, Yamada S, Kurimoto K, Tanabe H, Hirabayashi S, Sonohara F, et al. miR-23b-3p plays an oncogenic role in hepatocellular carcinoma. Ann Surg Oncol. 2021;28:3416–26. https://doi.org/10.1245/s10434-020-09283-y.
32. Dong S-S, Dong D-D, Yang Z-F, Zhu G-Q, Gao D-M, Chen J, et al. Exosomal miR-3682-3p suppresses angiogenesis by targeting ANGPT1 via the RAS-MEK1/2-ERK1/2 pathway in hepatocellular carcinoma. Front Cell Dev Biol. 2021;9. https://doi.org/10.3389/fcell.2021.633358.
33. Yadav N, Babu D, Madigubba S, Panigrahi M, Phanithi PB. Tyrphostin A9 attenuates glioblastoma growth by suppressing PYK2/EGFR-ERK signaling pathway. J Neurooncol. 2023;163:675–92. https://doi.org/10.1007/s11060-023-04383-7.

Publisher's note